Water Oxidation Hot Paper

Deutsche Ausgabe: DOI: 10.1002/ange.201411625
Internationale Ausgabe: DOI: 10.1002/anie.201411625

Electrocatalytic Water Oxidation by a Dinuclear Copper Complex in a Neutral Aqueous Solution**

Xiao-Jun Su, Meng Gao, Lei Jiao, Rong-Zhen Liao, Per E. M. Siegbahn, Jin-Pei Cheng, and Ming-Tian Zhang**

Abstract: *Electrocatalytic water oxidation using the oxidatively robust 2,7-[bis(2-pyridylmethyl)aminomethyl]-1,8-naphthyridine ligand (BPMAN)-based dinuclear copper(II) complex, $[Cu_2(BPMAN)(\mu\text{-}OH)]^{3+}$, has been investigated. This catalyst exhibits high reactivity and stability towards water oxidation in neutral aqueous solutions. DFT calculations suggest that the O–O bond formation takes place by an intramolecular direct coupling mechanism rather than by a nucleophilic attack of water on the high-oxidation-state Cu^{IV}=O moiety.*

The oxidation of water to oxygen, $2H_2O \rightarrow O_2 + 4H^+ + 4e^-$, is a key step for capturing solar energy in nature.[1] Developing molecular catalysts that can split water into oxygen and hydrogen is one of the main bottlenecks inhibiting the development of an effective and robust artificial photosynthetic system. Although a large body of molecular transition-metal catalysts and active metal oxide materials have been developed for water oxidation, substantial challenges remain for the ultimate goal of an efficient, inexpensive, and robust electro/photocatalyst.[2] Recently, copper-based water oxidation catalysts have become promising candidates because of their relatively high reactivity and stability and relatively low light absorption.[3] However, electrochemical water oxidation using these copper complexes usually involves alkaline conditions (pH > 10.8) rather than a neutral aqueous solution. Herein, we report an oxidatively stable dinuclear copper-based catalyst (Figure 1), $[Cu_2(BPMAN)(\mu\text{-}OH)]^{3+}$, which efficiently catalyzes water oxidation at a neutral pH without decomposition during long-term electrolysis.

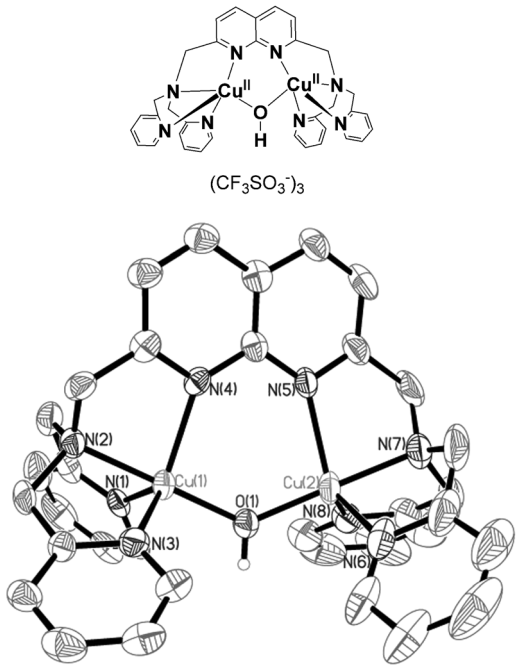

Figure 1. Top: The structure of the dicopper(II) catalyst, $[Cu_2(BPMAN)(\mu\text{-}OH)]^{3+}(OTf)_3$. Bottom: ORTEP view (thermal ellipsoids set at 50% probability) of the cation of $[Cu_2(BPMAN)(\mu\text{-}OH)]^{3+}$. The counter-anions and hydrogen atoms are omitted for clarity. Selected bond lengths [Å] and angles [°]: Cu(1)–O(1) 1.883(4), Cu(1)–N(1) 2.062(5), Cu(1)–N(2) 2.009(5), Cu(1)–N(3) 2.099(5), Cu(1)–N(4) 2.200(5), Cu(2)–O(1) 1.864(4), Cu(2)–N(5) 2.201(5), Cu(2)–N(6) 2.073(7), Cu(2)–N(7) 2.004(6), Cu(2)–N(8) 2.085(6); Cu1-O1-Cu2 131.7(2).

A 1,8-naphthyridine-based ligand, 2,7-[bis(2-pyridylmethyl)aminomethyl]-1,8-naphthyridine (BPMAN), was synthesized and used as a bis-TPA dinucleating ligand.[4,5] The dicopper(II) compound was prepared by treating one equivalent of the BPMAN ligand with two equivalents of $Cu^{II}(CF_3SO_3)_2$ and was recrystallized from ethanol/H_2O. The X-ray crystal structure shows that the complex consists of one $[Cu_2(BPMAN)(\mu\text{-}OH)]^{3+}$ cation (Figure 1), three trifluomethanesulfonate ($CF_3SO_3^-$) ions, and a water molecule. The copper atoms, Cu(1) and Cu(2), are separated by 3.4 Å and linked by an OH ion. The two Cu–(μ-OH) bonds are 1.883(4) Å and 1.864(4) Å. The Cu(1)-O-Cu(2) angle is 131.7(2)°. Both copper atoms are coordinated to four N

[*] X.-J. Su, M. Gao, Prof. Dr. L. Jiao, Prof. Dr. J.-P. Cheng, Prof. Dr. M.-T. Zhang
Center of Basic Molecular Science (CBMS)
Department of Chemistry
Tsinghua University
Beijing 100084 (China)
E-mail: mtzhang@mail.tsinghua.edu.cn
Prof. Dr. R.-Z. Liao
Key Laboratory for Large-Format Battery Materials and System
Ministry of Education
School of Chemistry and Chemical Engineering
Huazhong University of Science and Technology
Wuhan 430074 (China)
E-mail: rongzhen@hust.edu.cn
Prof. P. E. M. Siegbahn
Department of Organic Chemistry, Arrhenius Laboratory
Stockholm University, Stockholm SE-10691 (Sweden)

[**] This work was supported by the National Natural Science Foundation of China (Grant No. 201313299379 and 20131080083) and National Program for Thousand Young Talents of China. Computer time was provided by the Swedish National Infrastructure for Computing.

Supporting information for this article is available on the WWW under http://dx.doi.org/10.1002/anie.201411625.

atoms of the BPMAN ligand and one bridging O atom. The magnetic properties of this compound were determined over the temperature range of 2–300 K. Plots of magnetic susceptibility χ_m^{-1} and $\chi_m T$ versus T are shown in the Supporting Information. The observed value of $\chi_m T$ at 300 K equals 0.73 $cm^{-3}\,mol^{-1}\,K$, which is close to the spin-only value for two noncoupled Cu^{II} ions ($\chi_m T = 0.749\ cm^3\,mol^{-1}\,K$). X-ray photoelectron spectroscopy (XPS) data shows that the valence state of both copper atoms is +2. ESI-HRMS peaks at m/z 231.7119 ($\{Cu_2(BPMAN)(\mu\text{-}OH)\}^{3+}$, $z=3$) and m/z 993.0420 ($\{Cu_2(BPMAN)(\mu\text{-}OH)\}^{+} + 2\,OTf^-$, $z=1$) suggest the compound exists in solution as a dicopper form. $[Cu_2(BPMAN)(\mu\text{-}OH)]^{3+}$ exhibits good solubility in both acetonitrile and water, and its UV/Vis absorption is linearly dependent on the catalyst concentration, which indicates that the complex exists as a single species in dinuclear form (Figure S1 in the Supporting Information). The UV/Vis spectrum for this catalyst remained unchanged in water (pH 7) for 5 days (Figure S2), which indicates that the $Cu_2^{II,II}$ species is stable under neutral conditions.

The redox properties of this complex were systematically investigated by cyclic voltammetry (CV) in a phosphate buffer solution using boron-doped diamond (BDD) and ITO as the working electrodes and a saturated calomel electrode as the reference electrode. To report the potentials versus a normal hydrogen electrode (NHE), 0.244 V was added to the measured potentials. A typical CV plot for $[Cu_2(BPMAN)(\mu\text{-}OH)]^{3+}$ at pH 7.0 in 0.1 M phosphate buffer using the BDD electrode is shown in Figure 2.

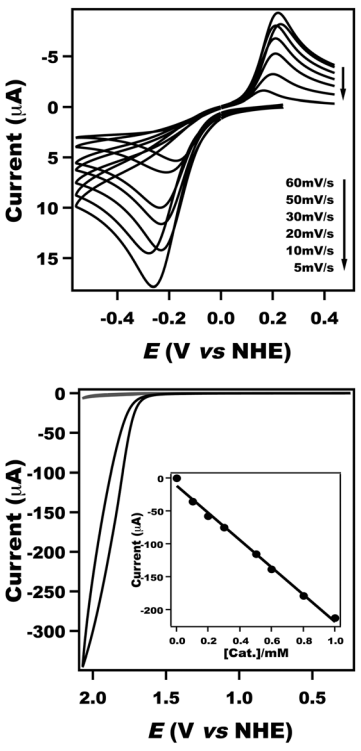

Figure 2. Top: CV of the $Cu_2^{II,II}/Cu_2^{I,II}$ couple during a negative scan (scan rate = 5 ~ 60 $mV\,s^{-1}$). Bottom: CV in 0.1 M phosphate buffer (pH 7.0) using a BDD electrode without (gray line) and with (black line) 1 mM $[Cu_2(BPMAN)(\mu\text{-}OH)]^{3+}$; the scan rate was 100 $mV\,s^{-1}$. Inset: Plot of the catalytic current at $E = 1.87$ V versus NHE as a function of the catalyst concentration.

An irreversible anodic wave at $E_{pc} = 0.18$ V versus NHE was observed in the CV, and an irreversible cathodic wave at $E_{pa} = -0.16$ V versus NHE was observed in the reverse scan (scan rate = 5 $mV\,s^{-1}$ (Figure 2 Top, with peak–peak splitting $\Delta E_p = 340$ mV). When the CV was measured using different scan rates, both of the peak currents varied linearly with the square root of the scan rate and the $Cu_2^{II,II}$ complex concentration, which indicates a diffusion-controlled process. The irreversible cathodic peak is pH dependent, with approximately −59 mV/pH unit (Figure S3). This kind of electrochemical behavior can be rationalized by the proton-coupled electron-transfer (PCET) reduction of $Cu_2^{II,II}$ to $Cu_2^{I,II}$, and DFT calculated potential for this process is, −0.12 V versus NHE, consistent with the measured values[6] (see Figures S4, S5, S14).

Under a positive potential, an irreversible oxidation wave appears at $E = 1.6$ V versus NHE (onset potential) and the potential for this process was 1.87 V versus NHE (this was determined by DPV method, see Supporting Information) in the 0.1 M phosphate buffer (pH 7.0). The catalytic current shown in Figure 2 inset, is considerably greater than that for the stoichiometric diffusion-controlled redox process. This is an electrocatalytic water-oxidation process as we will discuss below. The onset potential for this catalytic current clearly depends on the solution pH value, with a slope of approximately −59 $mV\,pH^{-1}$ (Figure S6), which is consistent with a PCET oxidation. The resulting complex may form an O–O bond and thus oxidize water, as will be discussed below. The overpotential was approximately 0.8 V at pH 7 in 0.1 M phosphate buffer. Catalytic water oxidation involving an uncomplexed Cu^{II} ion was ruled out using control experiments (Figure S7).

The oxygen evolution was investigated using controlled-potential electrolysis at 1.87 V versus NHE with a large-surface-area ITO electrode (1.5 cm^2) and a 1 mM $Cu_2^{II,II}$ complex in 0.1 M phosphate buffer (pH 7.0; Figure 3). The oxygen formed in the solution was measured using a calibrated Ocean Optics FOXY probe (Figure 3). The background O_2 formation without the copper catalyst was negligibly small. The use of a 1 mM dicopper catalyst maintained the catalytic current density at 0.4 $mA\,cm^{-2}$ for approximately 0.5 h during the electrolysis, and the O_2 dissolved in the solution phase increased from 10 μM to approximately 200 μM with a Faraday efficiency of around 98 % for the O_2 evolution.

During this long-term electrolysis of up to 4 h, no spectroscopic change was observed (Figure S8), which indicates that the major part of the catalyst was unchanged. No evidence of heterogeneity in the catalyst was detected (Figure S9, S10), and no significant changes in the peak currents or wave shape after multiple CVs and during the controlled-potential electrolysis (Figure S11) were observed. A BDD electrode previously subjected to the catalytic water-oxidation electrolysis at 1.87 V versus NHE with an approximately 1 mM $Cu_2^{II,II}$ catalyst at pH 7 for 2 h, exhibited no catalytic response in a fresh copper-catalyst-free electrolyte at pH 7 (Figure S12). Thus, these data are consistent with

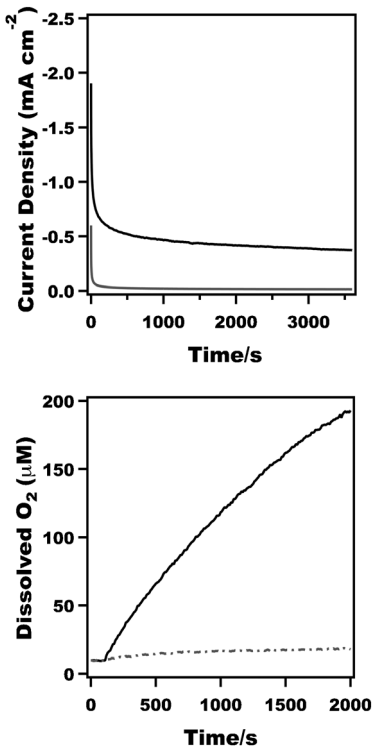

Figure 3. Top: Bulk electrolysis with (black line) and without (gray line) the $Cu_2^{II,II}$ catalyst (1 mM) at an ITO electrode in 0.1 M phosphate buffer (pH 7.0) at 1.87 V versus NHE. Bottom: The O_2 evolution during the bulk electrolysis without (gray line) and with (black line) the $Cu_2^{II,II}$ catalyst (1 mM), as measured with a fluorescence probe.

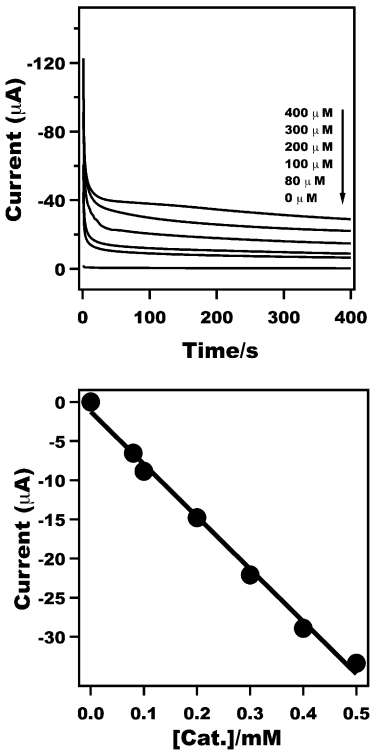

Figure 4. Top: Controlled potential electrolysis for differing concentrations of the catalyst in 0.1 M phosphate buffer, pH 7.0, using a boron-doped diamond (BDD) electrode (0.07 cm^2) at 1.87 V versus NHE. Bottom: plot of i_{cat} (minus the background current) versus $[Cu_2]$ in 0.1 M phosphate buffer at pH 7.0.

a homogeneous catalytic process for the conditions used, despite the difficulty of definitively excluding a colloid material.

To explore this catalytic process in detail, we investigated the water-oxidation kinetics of the $Cu_2^{II,II}$ catalyst as a function of its concentration, $[Cu_2]$, by controlling the electrolysis measurements to obtain the steady-state catalytic current, i_{cat}. The electrode potential was maintained at 1.87 V versus NHE for an unstirred solution, where i_{cat} is the initial plateau current (400 s) for a solution with a different $[Cu_2]$, as shown in Figure 4.

The catalytic current for water oxidation in the CV measurements varied linearly with the catalyst concentration (Figure 2, inset); therefore, the catalytic rate constants ($k_{cat.}$) can be expressed as $i_{cat.}$ using Equation (1 a), where $n_{cat.} = 4$ is

$$i_{cat.} = n_{cat.} F A\,[Cu_2] D_{Cu_2}{}^{1/2}\, k_{cat.}{}^{1/2} \quad (1a)$$

the electrochemical stoichiometry for water oxidation, F is the Faraday constant (96485.3 C), A is the electrode surface area (in cm^2, 0.07 cm^2 for BDD electrode used here), v is the scan rate, $[Cu_2]$ is the concentration of catalyst (in mol L^{-1}), α (= 0.5) was known as transfer coefficient and D_{Cu^2} (3.48×10^{-5} $cm^2 s^{-1}$) is the catalyst diffusion coefficient in the 0.1 M phosphate buffer at pH 7.0. D_{Cu^2} was determined from the scan-rate-dependent CV measurements of the $Cu_2^{II,II}/Cu_2^{I,II}$ couple using Equation (1 b) (Figure S13).[7]

$$i_d = 0.496\alpha^{1/2} F A\,[Cu_2]\,(F v D_{Cu_2}/RT)^{1/2} \quad (1b)$$

The steady-state catalytic current, $i_{cat.}$, is proportional to $[Cu_2]$, which is also consistent with Equation (1 a). The parameter $k_{cat.}$ in the case of a 0.1 M phosphate buffer solution at pH 7.0 was determined to be 0.6 s^{-1} on the basis of Equation (1 a). This value is comparable to those of most reported molecular water-oxidation catalysts.[8] The calculated $k_{cat.}$ value of the complicated $4e^-$ water oxidation catalytic process serves only as an estimate of the catalytic rate relative to the simple electrochemical model of catalytic regeneration of electroactive species in a following homogeneous reaction ($E_rC_{cat.}$).

Despite the important progress achieved in the field of water-oxidation catalysis, describing the catalytic mechanism is still a formidable challenge. Generally, the O–O bond formation may occur by an O-atom transfer to a water molecule (i.e., a water nucleophilic attack pathway)[9] or the coupling of two M^n=O centers in the specific case of Ru^{IV}=O complexes.[2e,10]

Considering the difficulty of unravelling the mechanistic details of this catalytic process solely on the basis of experiments, we performed DFT calculations to gain insights into the catalytic cycle (Figures 5 and 6). All the intermediates including their different protonated states and all the possible isomers have been calculated to identify the most stable structures under the working conditions (pH 7.0). For the redox potential of the water oxidation (pH 7), DFT calcu-

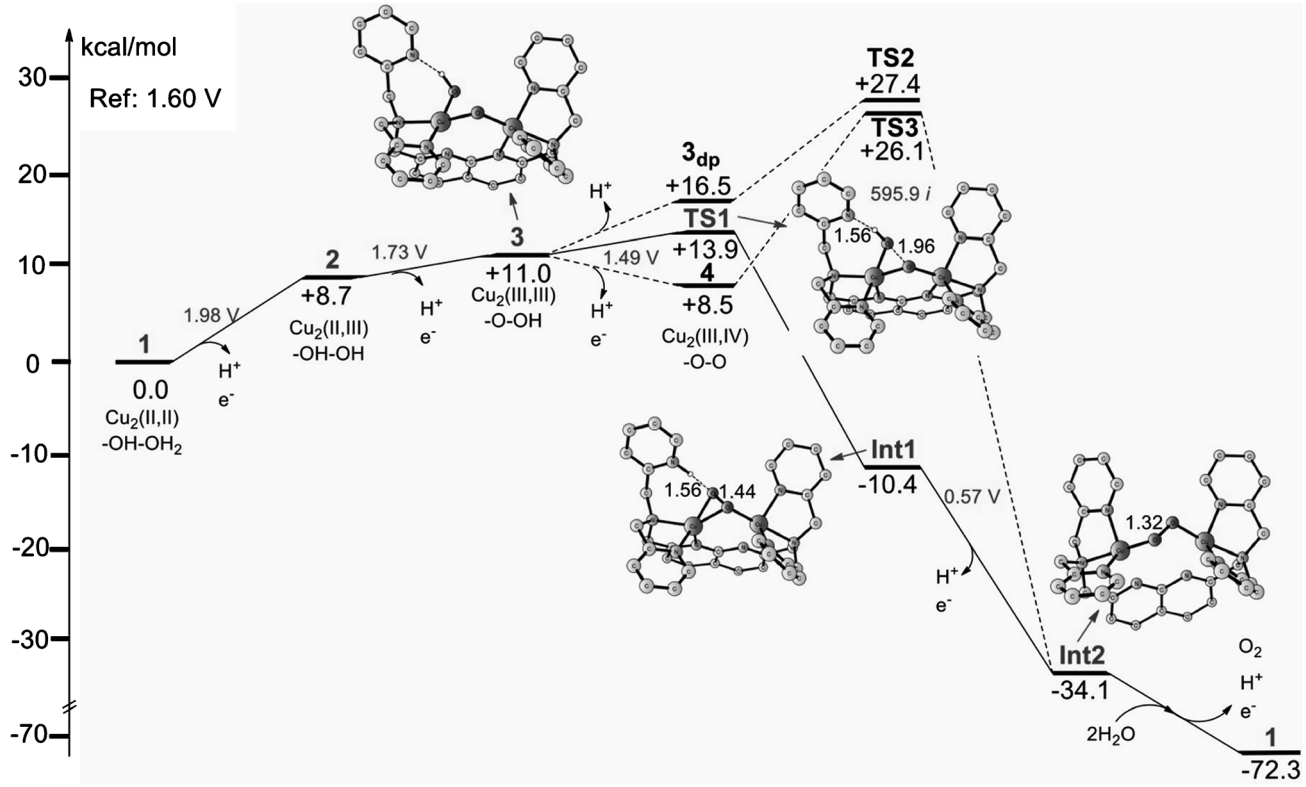

Figure 5. Energy diagram ($\Delta G_{298\,K}$ in kcal mol^{-1}) for water oxidation catalyzed by **1**. The reference potential of 1.6 V is used to set up the thermodynamics. Optimized structures of the intermediates **3**, **TS1**, **Int1**, and **Int2** are shown. For clarity, unimportant hydrogen atoms are not shown. The imaginary frequency of **TS1** is indicated. For structures of other intermediates, see Supporting Information.

lations (B3LYP*) gave a value of 0.73 V. Compared with the experimental value, the error is 0.086 V, or 2.0 kcal mol^{-1}. Four oxidation steps are involved in each catalytic cycle thus the error for the driving force, derived from the difference between the applied potential and the potential for water oxidation, is 4×2.0 kcal mol^{-1}, or 8.0 kcal mol^{-1}. To get the correct driving force, a correction is added for each oxidation, in which 0.086 V is added for the redox potential obtained by DFT calculations. This kind of methodology has been applied in a number of water-oxidation catalysts (see Supporting Information).

The most likely structure of the catalyst (pH 7.0) was first investigated and has been identified as **1** after calculating a large number of possible isomers (Figures S14–S16).[11] When $[Cu_2(BPMAN)(\mu\text{-}OH)]^{3+}$ is dissolved in water, a water molecule becomes coordinated to one Cu center. In the meantime, one pyridyl group dissociates from the corresponding Cu center and interacts with the entering water molecule by a hydrogen bond. The resulting $Cu_2^{II,II}$ complex **1** is oxidized through a PCET to yield a $Cu_2^{II,III}$ complex **2** (Figures 5, 6, S17 and S18), which can be further oxidized to a $Cu_2^{III,III}$ complex **3** by PCET (Figure 5, 6, S19, S20). The redox potentials for these two steps were calculated to be 1.98 V and 1.73 V versus NHE, respectively. Since the potential for the second step was 0.25 V lower, a $2e^- + 2H^+$ direct oxidation from complex **1** to complex **3** is possible. This result is in full accordance with the observation that the catalytic process takes place on the electrode showing −59 mV/pH unit dependence (Figure S6). Three possible pathways can be envisioned for the O−O bond formation from the $Cu_2^{III,III}$ complex **3** (Figure 5): First, the O−O bond can be formed directly via **TS1** (Figure S21), which is coupled with intramolecular proton transfer from the hydroxide to the pyridyl nitrogen (**3**→**Int1**). The barrier was calculated to be only 2.9 kcal mol^{-1} relative to **3** (Figure 5), and the total barrier became 13.9 kcal mol^{-1} if the energetic penalty for the generation of **3** is added (reference potential of 1.6 V). The electronic structure of the resulting **Int1** can be described as a triplet $Cu_2^{II,II}$ peroxide, which can be easily oxidized to **Int2** coupled with the release of one proton. **Int2** is a $Cu_2^{II,II}$ superoxide (Figure S22), and this kind of peroxo- (superoxo-) bridged dicopper complex has been extensively investigated in the Cu_n/O_2 bioinorganic systems and also plays an important role in making or breaking dioxygen O−O bonds in natural and artificial copper systems.[12–14] Second, complex **3** (pK_a of 11.0) could get deprotonated, first to form complex $\mathbf{3_{dp}}$ (Figure 5) which then converts into a classic peroxo-bridged $Cu_2^{II,II}$ peroxide complex, $\mathbf{Int1_{dp}}$ (Figure S23). However, the total barrier for this pathway (27.4 kcal mol^{-1}) was calculated to be 12.5 kcal mol^{-1} higher than the first pathway via **TS1** (13.9 kcal mol^{-1}, Figure 5); Third, complex **3** could undergo PCET to form the $Cu_2^{III,IV}$ complex **4** that has two μ-oxo bridges (via **TS2**, Figure S24). Then **4** could initiate O−O bond formation by a coupling of the two oxo groups via **TS3** to generate **Int2**. This pathway has a barrier of 26.1 kcal mol^{-1}, which is much higher than the first pathway (Figure S25). On

the basis of these calculations, the first scenario (**3**→**Int1**→**Int2**, as shown in Figures 5 and 6) is proposed to be the most likely pathway for O–O bond formation enabled by the present catalyst, in which the cooperation of two Cu centers plays a vital role. Importantly, this dinuclear Cu^{II} catalyst avoids the access of the high-oxidation state, Cu^{IV}=O. The best pathway for Cu^{IV}=O is a nucleophilic water attack on the oxo group, as in the case of Cu^{II} polypeptide catalyst reported by Meyer et al.,[3b] but this pathway is not preferred in the present case. This is also different from the very recent proposal of water-oxidation catalyzed by mononuclear Cu bicarbonate complex, in which O–O bond formation takes place by coupling of Cu^{IV}-OH and carbonate.[15]

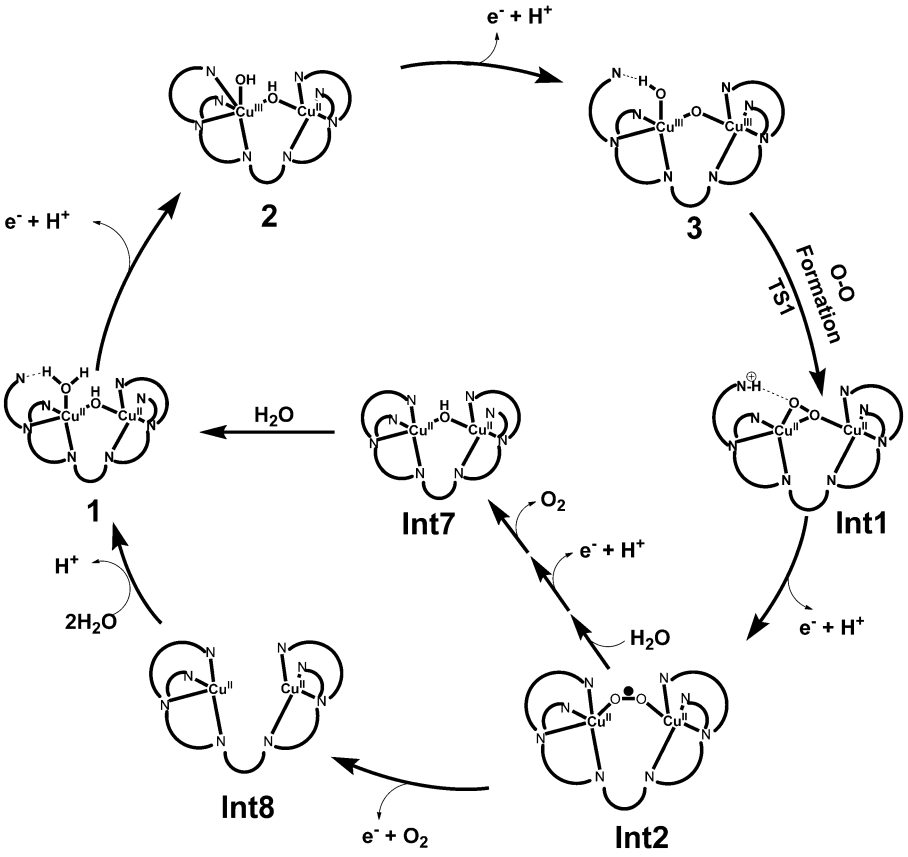

Figure 6. Proposed water-oxidation mechanism using $[Cu_2(BPMAN)(\mu\text{-}OH)]^{3+}$ in 0.1 M phosphate buffer at pH 7.0.

We further investigated the O_2 release from **Int2** using DFT calculations (Figure S26–S31).[16] Three possibilities have been considered. First, the direct release of O_2 from **Int2** prior to oxidation via **TS4** and **TS5** (Figure S27, S28), the barrier was calculated to be 16.2 kcal mol^{-1}. This leads to the formation of a $Cu_2^{I,II}$ complex **Int4** (Figure S28), which can undergo one-electron oxidation, followed by binding of two water molecules, and release of one proton to regenerate **1**. Second, **Int2** could bind a water molecule to form **Int5**, which is slightly exergonic by 0.2 kcal mol^{-1} (Figure S29). This is then followed by a very facile O_2 dissociation from one Cu center to form **Int6**, in which O_2 coordinates to one Cu in an end-on fashion. **Int6** can be further oxidized (−0.14 V vs. NHE) to release O_2 and form **Int7**, which can be converted into complex **1** by the binding of one water molecule to start the next catalytic cycle (Figure S30). Third, **Int2** could undergo one-electron oxidation directly (0.79 V vs. NHE) concomitant with O_2 evolution to form **Int8** (Figure S31), which can be converted easily into **1**. Since it is very difficult to calculate the rate for the oxidation during the O_2 evolution for these three pathways, we cannot make a definite conclusion about which one is preferred but it seems that all three pathways may contribute.

Based on our combined experimental and computational study, a most likely and plausible mechanism for $[Cu_2(BPMAN)(\mu\text{-}OH)]^{3+}$-catalyzed water oxidation is proposed and shown in Figure 6. $[Cu_2(BPMAN)(\mu\text{-}OH)]^{3+}$ exists as complex **1** under working conditions of the solution (pH 7.0), and complex **1** is oxidized through two consecutive PCETs to give complex **3**. Then the intramolecular proton transfer of complex **3** triggers the O–O bond formation through the coupling between Cu^{III}–O(H) and a μ-oxo to form **Int1** which is further oxidized to **Int2**, a $Cu_2^{II,II}$ superoxide. This superoxide bridged dicopper intermediate, is further oxidized to release O_2 and starts the next catalytic cycle. This mechanism is different from the common pathway of O–O bond formation by nucleophilic water attack on the high-oxidation-state M^{n+}=O moiety, and also avoids the high oxidation state of Cu^{IV}=O that has been proposed to initiate O–O bond formation and also hydrocarbon oxidation.[17] The O–O bond formation mechanism reported herein provides a new way to enable O–O bond formation and to tour knowledge, a similar pathway has not been reported to date.

We have reported a robust dinuclear Cu complex and carefully investigated its catalytic performance for water oxidation. Importantly, this is the first copper-based molecular water-oxidation catalyst used in a neutral aqueous solution. DFT calculations revealed that O–O bond formation proceeds by a cooperative interaction between two Cu^{III} centers rather than by the high-oxidation-state Cu^{IV}=O moiety reported for a Cu^{II} peptide catalyst.[3b] Further experiments are in progress to improve the catalyst by reducing its high overpotential, in particular.

Keywords: copper · homogeneous catalysis · O–O coupling · superoxide complexes · water oxidation

How to cite: *Angew. Chem. Int. Ed.* **2015**, *54*, 4909 – 4914
Angew. Chem. **2015**, *127*, 4991 – 4996

[1] a) F. Liu, J. J. Concepcion, J. W. Jurss, T. Cardolaccia, J. L. Templeton, T. J. Meyer, *Inorg. Chem.* **2008**, *47*, 1727 – 1752; b) R. Eisenberg, H. B. Gray, *Inorg. Chem.* **2008**, *47*, 1697 – 1699; c) J. K. Hurst, *Science* **2010**, *328*, 315 – 316; d) N. Cox, D. A. Pantazis, F. Neese, W. Lubitz, *Acc. Chem. Res.* **2013**, *46*, 1588 – 1596.

[2] a) X. Liu, F. Y. Wang, *Coord. Chem. Rev.* **2012**, *256*, 1115 – 1136; b) B. Limburg, E. Bouwman, S. Bonnet, *Coord. Chem. Rev.* **2012**, *256*, 1451 – 1467; c) D. J. Wasylenko, R. D. Palmer, C. P. Berlinguette, *Chem. Commun.* **2013**, *49*, 218 – 227; d) D. G. H. Hetterscheid, J. N. H. Reek, *Angew. Chem. Int. Ed.* **2012**, *51*, 9740 – 9747; *Angew. Chem.* **2012**, *124*, 9878 – 9885; e) X. Sala, S. Maji, R. Bofill, J. Garcia-Anton, L. Escriche, A. Llobet, *Acc. Chem. Res.* **2014**, *47*, 504 – 516; f) M. D. Kärkäs, E. V. Johnston, O. Verho, B. Akermark, *Acc. Chem. Res.* **2014**, *47*, 100 – 111.

[3] a) S. M. Barnett, K. I. Goldberg, J. M. Mayer, *Nat. Chem.* **2012**, *4*, 498 – 502; b) M.-T. Zhang, Z. F. Chen, P. Kang, T. J. Meyer, *J. Am. Chem. Soc.* **2013**, *135*, 2048 – 2051; c) Z. Chen, P. Kang, M.-T. Zhang, B. R. Stoner, T. J. Meyer, *Energy Environ. Sci.* **2013**, *6*, 813 – 817; d) Z. Chen, T. J. Meyer, *Angew. Chem. Int. Ed.* **2013**, *52*, 700 – 703; *Angew. Chem.* **2013**, *125*, 728 – 731; e) M. K. Coggins, M. T. Zhang, N. Song, T. J. Meyer, *Angew. Chem. Int. Ed.* **2014**, *53*, 12226 – 12230; *Angew. Chem.* **2014**, *126*, 12422 – 12426; f) T. Zhang, C. Wang, S. B. Liu, J. L. Wang, W. B. Lin, *J. Am. Chem. Soc.* **2014**, *136*, 273 – 281.

[4] a) C. He, S. J. Lippard, *Tetrahedron* **2000**, *56*, 8245 – 8252; b) C. Vu, D. Walker, J. Wells, S. Fox, *J. Heterocycl. Chem.* **2002**, *39*, 829 – 832.

[5] C. He, J. L. DuBois, B. Hedman, K. O. Hodgson, S. J. Lippard, *Angew. Chem. Int. Ed.* **2001**, *40*, 1484 – 1487; *Angew. Chem.* **2001**, *113*, 1532 – 1535.

[6] For more details, see Supporting Information.

[7] a) A. J. Bard, L. R. Faulkner, *Electrochemical methods*: *Fundamentals and applications*, *2nd ed.*, Wiley, New York, **2001**, p. 235 and A. J. Bard, L. R. Faulkner, *Electrochemical methods*: *Fundamentals and applications*, *2nd ed.*, Wiley, New York, **2001**, p. 501; b) R. G. Compton, C. E. Banks, *Understanding Voltammetry*, *2nd ed.*, Imperial College Press, London, **2011**, p. 121; c) Z. Chen, C. Chen, D. Weinberg, P. Kang, J. J. Concepcion, D. Harrison, M. Brookhart, T. J. Meyer, *Chem. Commun.* **2011**, *47*, 12607 – 12609.

[8] a) W. C. Ellis, N. D. McDaniel, S. Bernhard, T. J. Collins, *J. Am. Chem. Soc.* **2010**, *132*, 10990 – 10991; b) M. K. Coggins, M. T. Zhang, A. K. Vannucci, C. J. Dares, T. J. Meyer, *J. Am. Chem. Soc.* **2014**, *136*, 5531 – 5534.

[9] Z. F. Chen, J. J. Concepcion, X. Q. Hu, W. T. Yang, P. G. Hoertz, T. J. Meyer, *Proc. Natl. Acad. Sci. USA* **2010**, *107*, 7225 – 7229.

[10] a) L. L. Duan, F. Bozoglian, S. Mandal, B. Stewart, T. Privalov, A. Llobet, L. C. Sun, *Nat. Chem.* **2012**, *4*, 418 – 423; b) J. Nyhlén, L. L. Duan, B, Akermark, L. C. Sun, T. Privalov, *Angew. Chem. Int. Ed.* **2010**, *49*, 1773 – 1777; *Angew. Chem.* **2010**, *122*, 1817 – 1821; c) S. Romain, F. Bozoglian, X. Sala, A. Llobet, *J. Am. Chem. Soc.* **2009**, *131*, 2768 – 2769; d) S. Maji, L. Vigara, F. Cottone, F. Bazoglian, J. Benet-Buchholz, A. Llobet, *Angew. Chem. Int. Ed.* **2012**, *51*, 5967 – 5970; *Angew. Chem.* **2012**, *124*, 6069 – 6072.

[11] Two control experiments, to some extent, can exclude the possibility of phosphate acts as a ligand binding to copper center: a) HR-MS of the catalyst dissolved in pure water was identical to the sample in 0.1 M phosphate buffer (Supporting Information); b) The catalytic current has a similar strength in different concentrations of buffer solution (0.02 M–2 M, pH 7, see Supporting Information).

[12] a) A. Crespo, M. A. Marti, A. E. Roitberg, L. M. Amzel, D. A. Estrin, *J. Am. Chem. Soc.* **2006**, *128*, 12817 – 12828; b) P. Chen, E. I. Solomon, *J. Am. Chem. Soc.* **2004**, *126*, 4991 – 5000.

[13] a) D. Maiti, H. R. Lucas, A. A. N. Sarjeant, K. D. Karlin, *J. Am. Chem. Soc.* **2007**, *129*, 6998 – 6999; b) N. Kitajima, T. Koda, Y. Iwata, Y. Morooka, *J. Am. Chem. Soc.* **1990**, *112*, 8833 – 8839; c) S. M. Huber, M. Z. Ertem, F. Aquilante, L. Gagliardi, W. B. Tolman, C. J. Cramer, *Chem. Eur. J.* **2009**, *15*, 4886 – 4895.

[14] a) E. A. Lewis, W. B. Tolman, *Chem. Rev.* **2004**, *104*, 1047 – 1076; b) L. M. Mirica, X. Ottenwaelder, T. D. P. Stack, *Chem. Rev.* **2004**, *104*, 1013 – 1046; c) E. I. Solomon, D. E. Heppner, E. M. Johnston, J. W. Ginsbach, J. Cirera, M. Qayyum, M. T. Kieber-Emmons, C. H. Kjaergaard, R. G. Hadt, L. Tian, *Chem. Rev.* **2014**, *114*, 3659 – 3853; d) M. T. Kieber-Emmons, J. W. Ginsbach, P. K. Wick, H. R. Lucas, M. E. Helton, B. Lucchese, M. Suzuki, A. D. Zuberbuhler, K. D. Karlin, E. I. Solomon, *Angew. Chem. Int. Ed.* **2014**, *53*, 4935 – 4939; *Angew. Chem.* **2014**, *126*, 5035 – 5039; e) N. Kindermann, E. Bill, S. Dechert, S. Demeshko, E. J. Reijerse, F. Meyer *Angew. Chem. Int. Ed.* **2015**, *54*, 1738 – 1743; *Angew. Chem.* **2015**, *127*, 1758 – 1763.

[15] S. G. Winikoff, C. J. Cramer, *Catal. Sci. Technol.* **2014**, *4*, 2484 – 2489.

[16] The energetic diagram and the optimized structures of intermediates and TS for oxygen evolution process are given in the Supporting Information.

[17] A. Conde, L. Vilella, D. Balcells, M. M. Díaz-Requejo, A. Lledós, P. J. Pérez, *J. Am. Chem. Soc.* **2013**, *135*, 3887 – 3896.

Received: December 2, 2014
Published online: February 10, 2015

